An exciton-phonon interaction model for singlet fission in prototypical molecular crystals

Xiaoyu Xie,[†] Alejandro Santana-Bonilla,[‡] Weihai Fang,[†,¶] Chungen Liu,[*,†] Alessandro Troisi,[*,‡] and Haibo Ma[*,†]

[†]*School of Chemistry and Chemical Engineering, Nanjing University, Nanjing 210023, China*

[‡]*Department of Chemistry, University of Liverpool, Liverpool L69 3BX, UK*

[¶]*Department of Chemistry, Beijing Normal University, Beijing, 100875, China*

E-mail: cgliu@nju.edu.cn; a.troisi@liverpool.ac.uk; haibo@nju.edu.cn

Abstract

In singlet fission (SF), a spin-conserving splitting of one singlet exciton into two triplet excitation states, the transition between localized electronic states can be controlled and modulated by delocalized lattice phonons. In this work, we built an exciton-phonon (ex-ph) interaction model accounting local electronic states coupled with both local molecular vibrations and low frequency intermolecular phonon modes for SF in crystalline tetracene and rubrene. On the basis of the calculated electronic couplings at the equilibrium structure of molecular dimer, a superexchange path for SF was found for tetracene while couplings between the triplet pair (TT) state and other diabatic states are zero for rubrene due to the high symmetry. Our further ex-ph spectral density analysis and quantum dynamics simulation based on our ex-ph interaction model suggested

a thermal-activated mechanism for SF in rubrene crystal via symmetry breaking by nuclear vibration, which is in agreement with recent experiments. It is also shown that thermal fluctuations of electronic couplings in both tetracene and rubrene are mostly in the same order of magnitude at room temperature, and this could be one of the reasons for both tetracene and rubrene to exhibit SF time scales within a close range (hundreds to thousands of femtoseconds) in experiments.

1 Introduction

Singlet fission is a spin-allowed photophysical process that generates two triplet excitons from one singlet excitation state in various organic materials including conjugated molecular crystal (oligoacenes, oligophenyls, etc.), conjugated polymers (polyenes, donor-acceptor polymers and so on) and covalent dimers/trimers.[1–10] SF was firstly proposed by Singh et al. to interpret the dark high-energy ^1A_g state as two coupled triplet excitons in anthracene crystal in 1965.[11] In the last decade, great interests on SF were revived after the work of Hanna and Nozik[12] which suggested multiple exciton generation (MEG) in organic semiconductors through SF to boost the power conversion efficiency (PCE) in solar cells by overcoming the Shockley-Queisser limit.[13]

Theoretical analysis can provide valuable insights to interpret experimental SF phenomena and to understand photophysical mechanisms. Firstly, numerous electronic structure calculations have been focused on the description the nature of the adiabatic or diabatic electronic excited states directly and indirectly involved in SF as well as the electronic coupling.[14–31] For conjugated molecular crystals and covalent oligomer systems, SF in a simplified molecular nearest-neighbor dimer (symbolize as AB) model is usually considered as an exciton dynamic process with transition from the initial local singlet excited states (LE states, A^*B/AB^*) to the triplet pair state (TT state or multi-exciton state ME state, A^TB^T),[14,32] and then the spin-coupled TT state splits into two free triplet excitons through Dexter energy transfer[33] mechanism. Since the direct two-electron coupling between LE

state and TT state has been found to be very weak in most systems, the intermediate charge transfer states (CT states, A^+B^-/A^-B^+) were also suggested to be mixed with singlet excitation states and donate an indirect coupling between LE and TT states.[34–36]

Secondly, besides the electronic couplings, the exciton-vibration (ex-vib) or exciton-phonon (ex-ph) couplings were also revealed as crucial to determine the SF rates in organic materials.[37–46] The local ex-ph couplings are dominated by the high frequency intramolecular vibration modes and contribute to the dynamic disorder of electronic state energies and the decoherence between electronic states. It was found that the couplings between the CT electronic states and intramolecular vibrational modes can significantly accelerate the SF process by enhancing the participation of CT states via the superexchange pathways.[40,41] On the other hand, low frequency intermolecular ex-ph couplings (nonlocal phonons interacting with LE-TT and CT-TT electronic couplings) are vital for activating the SF in rubrene crystal[39,47] via vibration-induced symmetry broken and these interaction could speed up SF rate through intermolecular[38] and intramolecular[44] modes. With the computed electronic and ex-vib or ex-ph couplings, real-time SF dynamics can be simulated using various theoretical schemes, including the full quantum dynamic approaches like the multiconfigurational time-dependent Hartree (MCTDH),[39,48,49] the time-dependent density matrix renormalization group (t-DMRG),[40] the stochastic Schrödinger equations (SSE) like time-dependent wavepacket diffusion method (TDWPD),[45] generalized quantum master equation,[38,42] and the mixed quantum-classical approaches such as the trajectory surface hopping (TSH),[50] etc.

Despite numerous computational works have made a substantial contribution to the understanding of SF, most of them employed the simplified dimer or oligomer model, which is obviously much distinct from the real crystals and in which the phonon modes are completely absent. The effect of the full set of realistic vibrational modes in the crystal on the SF process has never been explored. In particular, non-local ex-ph coupling is expected to be important for low frequency intermolecular modes, which cannot be studied accurately

from dimer models. Our recent work[51] indicated that sampling of phonon q-space could be a useful strategy to obtain the full information of vibration structure of crystalline system. And the crucial role of low frequency phonon modes was also revealed for the fluctuation of electronic couplings in the charge transfer process in organic molecular aggregates by our calculations. Additionally, the phonon structure analysis and spectral density results indicate that molecular packing not only affects the electronic couplings between monomers but also the detailed composition of nonlocal ex-ph couplings. Therefore, a theoretical work with the consideration of all local and nonlocal phonon modes in a realistic crystal environment would be very important for the quantitative description of the SF process and complement the widely used dimer and oligomer approaches.

In this work, we built an ex-ph interaction model accounting local electronic states coupled with both local molecular vibrations and low frequency intermolecular phonon modes for SF in two prototypical crystal systems, which are tetracene and rubrene as shown in Figure 1. These two molecules have the same core skeleton, and both of them undergo SF but with different microscopic mechanisms because the transition in one of them (rubrene) is symmetry forbidden.[47,52] Therefore, they offer a good set of molecular model systems to study electronic and phonon effects separately. All the model parameters were derived from (i) complete active space (CAS) electronic structure calculation for the dimers in Figure 1, (ii) a relatively accurate phonon structure by density functional tight-binding (DFTB) calculation, and (iii) all of the local and nonlocal ex-ph couplings obtained using our newly developed projection technique.[51] This general model provides a quantitative framework for the computational study for SF in molecular crystalline environments.

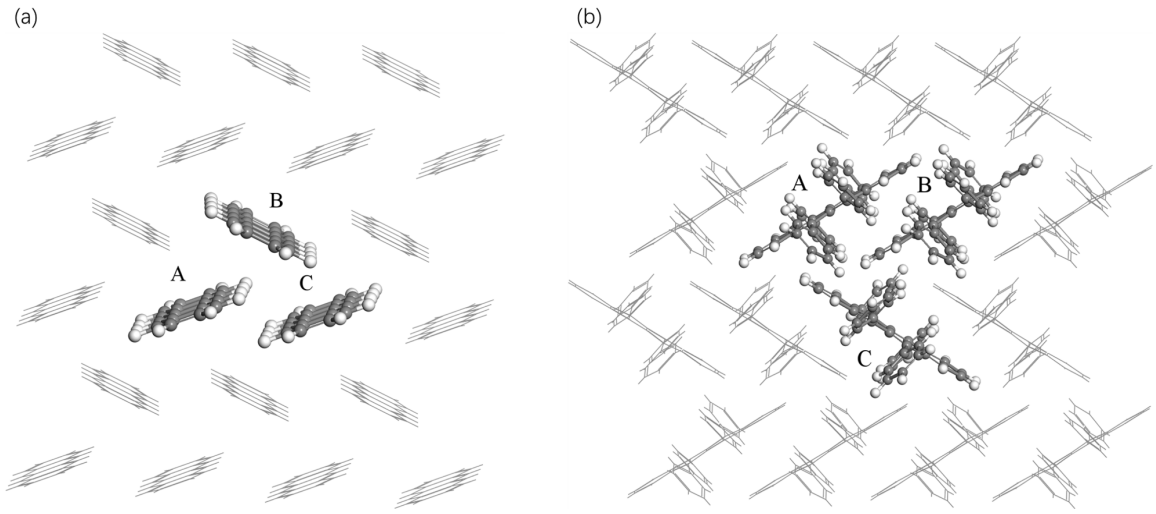

Figure 1: The selected dimers in (a) the *ab* layer of tetracene (with indexes AB, indexes AC and indexes BC) and (b) the *bc* layer of rubrene crystal (we only considered dimer AB as the interaction of local frontier molecular orbitals of dimer AC are very weak). Based on the dimers in these two crystalline systems, we constructed localized LE, CT and TT states.

2 Methodology and computational details

2.1 Diabatic electronic states for singlet fission

Three crucial electronic state groups are widely considered to be involved directly or indirectly in SF process: local excited (LE) state, charge transfer (CT) state and triplet pair (TT) state. The local feature of these three types of states allows us to study the electronic structure features of SF with a simplified model dimer system. As shown in Figure 2 with a molecular dimer AB, a diabatic electronic Hamiltonian can be built for SF investigation based on five spin-conservation diabatic states, which are two LE states (A^*B and AB^* labeled as LE1 and LE2), two CT states (A^+B^- and A^-B^+ named CT1 and CT2) and one TT state (A^TB^T).

In this work, tetracene and rubrene crystal systems were used to investigate the SF in crystalline system, and the electronic structure of selected dimers (as shown in Figure 1) were calculated.

Because of the multi-excitation feature of the TT state, multi-configuration wavefunction

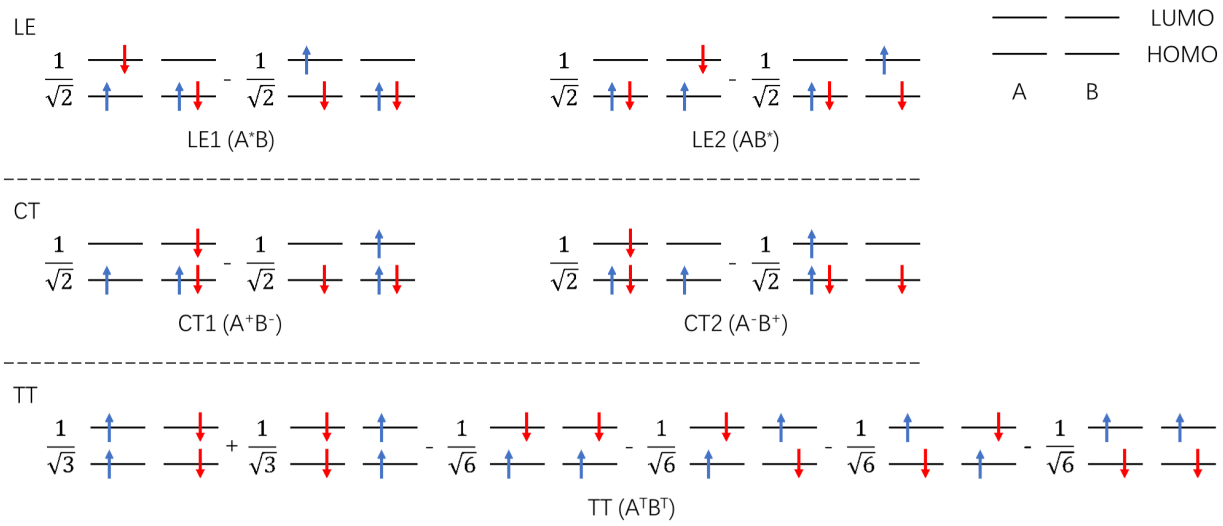

Figure 2: Diabatic states of SF in the dimer system. A and B represent two monomers of the dimer system. Black lines are localized HOMOs/ LUMOs, and red and blue arrows denote alpha- and beta-spin electrons respectively.

methods are necessary for characterising these excitation states. The complete active space configuration interaction (CASCI) and self-consistent field (CASSCF) calculations were performed using OpenMOLCAS package[53] in our calculations. Since plenty of many single point electronic structure calculations at different geometries are necessary for the later derivation of ex-ph couplings, here a minimal CAS configuration space, CAS(4e, 4o) was applied for the dimer systems as a good compromise between accuracy and computational cost. Previous works have shown that CAS calculations with a minimal active space can already capture the main electronic features in SF.[17] Then the wavefunctions of these five spin-conservation diabatic states (two LE states, two CT states and one TT state) which are built based on local highest occupied molecular orbitals (HOMOs)/ lowest unoccupied molecular orbitals (LUMOs) of monomers (Figure 2) could be expressed as linear combinations of adiabatic states Φ_a in the configuration space,

$$\Psi_i = \sum_a c_{ia} \Phi_a \tag{1}$$

where the coefficients c_{ia} can be obtained as the overlap integral between calculated adiabatic states Φ_a and diabatic states Ψ_i. Then, the energies of the diabatic states and their electronic couplings can be calculated by

$$\varepsilon_i = \langle \Psi_i | \hat{H} | \Psi_i \rangle = \sum_i |c_{ia}|^2 E_a \tag{2}$$

$$V_{ij} = \langle \Psi_i | \hat{H} | \Psi_j \rangle = \sum_i c_{ia}^* c_{ja} E_a \tag{3}$$

where E_a is the energy of adiabatic state Φ_a.

In practice, CASSCF/6-31G with (2e,2o) active space was used for each monomer of the dimer system, and with Löwdin orthogonalization method,[54] the localized orthonormal set $\{\varphi^{\mathrm{LO}}\}$ can be constructed based on the molecular orbital set $\{\phi\}$ of monomers,

$$\varphi^{\mathrm{LO}} = \mathbf{S}^{-\frac{1}{2}} \phi \tag{4}$$

here $\mathbf{S}$ is the overlap matrix of set $\{\phi\}$. And CASCI(4e, 4o)/6-31G(d) calculations were performed with the localized orthonormal set $\{\varphi^{\mathrm{LO}}\}$ to compute the wavefunctions of adiabatic states Φ_a for the molecular dimers.

2.2 Exciton-phonon interaction Hamiltonian model

To include the phonon effect into time evolution of electronic states for SF, a linear ex-ph interaction Hamiltonian could be constructed as,

$$\hat{H} = \hat{H}_{el} + \hat{H}_{ph} + \hat{H}_{ex-ph} \tag{5}$$

with

$$\hat{H}_{el} = \sum_i \varepsilon_i^0 |\Psi_i\rangle\langle\Psi_i| + \sum_{i \neq j} V_{ij}^0 |\Psi_i\rangle\langle\Psi_j|,$$

$$\hat{H}_{ph} = \sum_{I} \frac{1}{2}\hbar\omega_I(-\frac{\partial^2}{\partial Q_I^2} + Q_I^2),$$

$$\hat{H}_{ex-ph} = \sum_{i,I} g_i^I Q_I |\Psi_i\rangle\langle\Psi_i| + \sum_{i\neq j,I} g_{ij}^I Q_I |\Psi_i\rangle\langle\Psi_j|.$$

Here, $|\Psi_i\rangle$ represents a given electronic state among the five diabatic states, ε_i^0 and V_{ij}^0 are the energy of electronic state and the electronic coupling between them under the equilibrium geometry respectively. ω_I is frequency of phonon mode I of the two crystalline systems which was obtained from the DFTB calculations in our recent work[51] and Q_I is the dimensionless displacement. In ex-ph coupling part, g_i^I is local ex-ph coupling while g_{ij}^I is the nonlocal one.

Following our recent work,[51] we calculated the nonlocal ex-ph couplings for SF,

$$g_{ij}^I = \nabla V_{ij} \cdot \mathbf{Q}_I^c, \tag{6}$$

where ∇V_{ij} is the gradient of electronic couplings with respect to the atomic displacement respectively, and $\mathbf{Q}_I^c$ is the Cartesian displacement of mode I. Similarly, we can define the gradient of energies $\nabla\varepsilon_i$ and calculate the local ex-ph coupling by the equation below,

$$g_i^I = \nabla\varepsilon_i \cdot \mathbf{Q}_I^c. \tag{7}$$

For the numerical derivation of each gradient component, we applied linear fitting with three different geometries (-Δx, 0 and Δx). i.e. the computation of gradient required 361 and 841 CASCI single-point calculations for tetracene and rubrene respectively, which are computationally expensive. To reduce the computational cost, we set all components of gradient with respect to atoms of phenyl side chain in rubrene to zero because all excited states are localized in the tetracene core and tests to validate this approximation are given in the Supporting Information (SI).

3 Results and discussion

3.1 Electronic Hamiltonian

First, we calculated the electronic Hamiltonian of SF for both tetracene and rubrene dimer systems using the experimental crystalline structures[55,56] as equilibrium structures (dimer AB, AC and BC for tetracene and dimer AB for rubrene cf. in Figure 1), and the results are listed in Table 1 and Table 2 for tetracene dimer AB and rubrene dimer AB individually. (Results of tetracene dimer AC and BC are provided in SI.)

Table 1: Electronic Hamiltonian elements for tetracene dimer AB (unit: eV)

	A^*B	AB^*	A^+B^-	A^-B^+	A^TB^T
A^*B	4.144				
AB^*	0.026	4.070			
A^+B^-	0.109	0.090	4.509		
A^-B^+	-0.092	-0.112	0.000	4.992	
A^TB^T	0.000	0.000	0.070	0.087	4.065

Table 2: Electronic Hamiltonian elements for rubrene dimer AB (unit: eV)

	A^*B	AB^*	A^+B^-	A^-B^+	A^TB^T
A^*B	4.018				
AB^*	0.058	4.017			
A^+B^-	-0.086	-0.168	5.043		
A^-B^+	0.168	0.086	0.000	5.042	
A^TB^T	0.000	0.000	0.000	0.000	4.006

The magnitudes of couplings are in close agreements with other theoretical results[19,34,39] while the diagonal energy elements have markedly differences from the results computed via constrained density functional method,[17] multi-state density functional method,[34] multi-configuration wavefunction with[19] or without[16,39] perturbation methods due to the lack of dynamic correlation energy in our CASCI and CASSCF calculations. But the energy difference between the singlet excitation states and TT state are comparable with those in

references, i.e. we assume that the dynamic correlation problem in our case only results in an energy shift and will not affect the correctness of gradients $\nabla\varepsilon$ and local ex-ph couplings. On the other hand, in our calculations, the coupling between the LE states and the TT state are found to be almost zero for tetracene. This finding differs with the results by Casanova[17] ($\sim$ 2.2 meV), but is in agreement with more recent works by Parker et al.[19] and Morrison et al.,[44] which also predicted almost zero couplings between LE states and TT state. As discussed in the recent review by Casanova,[3] the distinction may be caused by the different approximations for the definition of diabatic states employed in different diabatization schemes.

Table 1 shows nonzero couplings (in magnitudes of tens or hundreds of meV) for both CT-LE and CT-TT pairs in tetracene, but coupling is negligible between the LE states and the TT state. This implies a superexchange path for SF[34–36] in the tetracene crystal. However, the electronic couplings between the TT state and the LE or the CT states are found to be zero for rubrene dimer AB (in Table 2). It should be noted that, such kind of zero electronic couplings within rubrene dimer AB are caused by its high structural symmetry (C_{2h}).[39,47] Therefore coherent SF can hardly happen under the equilibrium molecular geometry due to the high symmetry crystal structure. Other effects should contribute to the SF in rubrene crystals, and will be discussed in the next subsection.

3.2 Ex-ph couplings

Considering the large number of vibrational modes in crystalline system (related to the number of sampling $\mathbf{q}$ points), the following definition of spectral density can be a convenient way to analyze the ex-ph coupling:

$$J_{i/ij}(\omega) = \frac{1}{2\hbar}\sum_I {g^I_{i/ij}}^2 \delta(\omega - \omega_I), \tag{8}$$

where the Dirac δ function is approximated by a Gaussian broadening distribution with $\sigma = 5$ cm^{-1}.

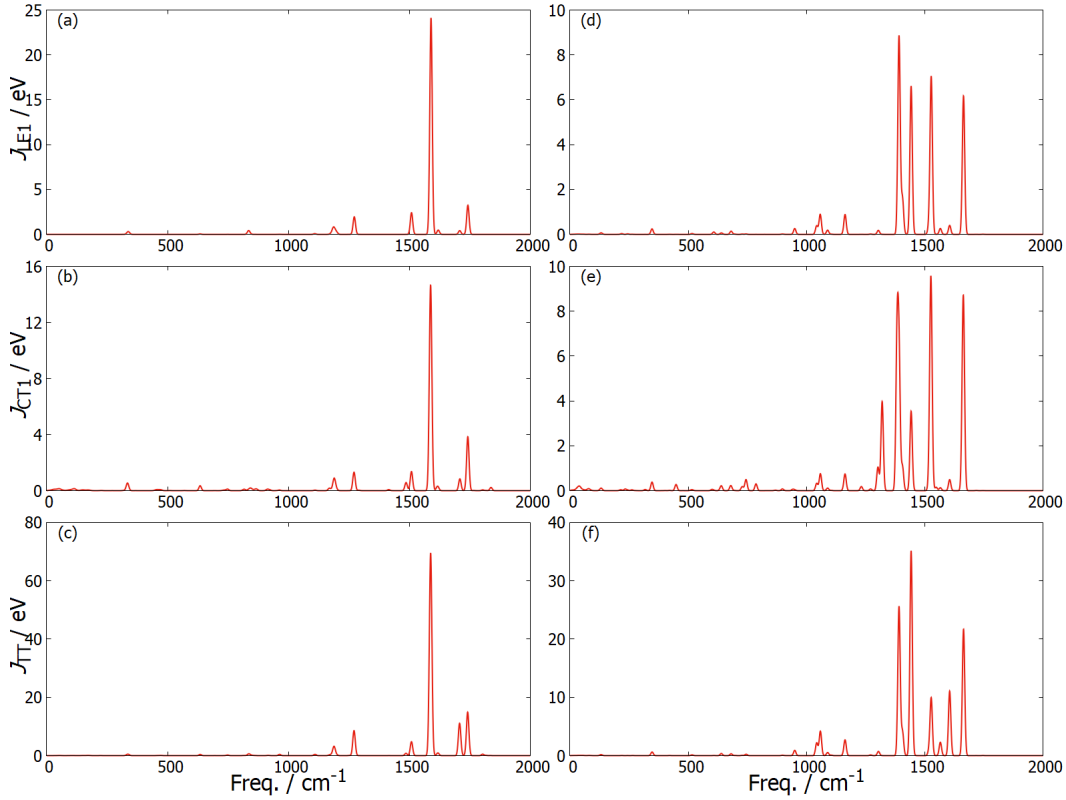

Figure 3: Spectral densities of local ex-ph couplings for tetracene dimer AB (a-c) with subfigures of (a) LE1 (A^*B) state, (b) CT1 (A^+B^-) state and (c) TT (A^TB^T) state, and rubrene dimer AB (d-f) with subfigures of (d) LE1 (A^*B) state, (e) CT1 (A^+B^-) state and (f) TT (A^TB^T) state.

Figure 3 and 4 illustrate the spectral densities of local ex-ph couplings and nonlocal ex-ph coupling results for tetracene dimer AB and rubrene dimer AB systems respectively (results of other tetracene dimers are displayed in SI). First, we computed the reorganization energy of rubrene using the spectral density of LE1 via $\lambda = \int \mathrm{d}\omega J(\omega)/\omega$, and our results is 330 meV, in the same order of magnitude with previous calculation results (159 meV).[57] In Figure 3 and 4, it is clearly shown that, for both systems, the local ex-ph interactions is dominated by high frequency (local molecular vibration) modes. At the same time, the non-local ex-ph interactions is mainly contributed by low frequency modes due to the large ex-ph couplings and higher occupation numbers of low frequency modes, but several high

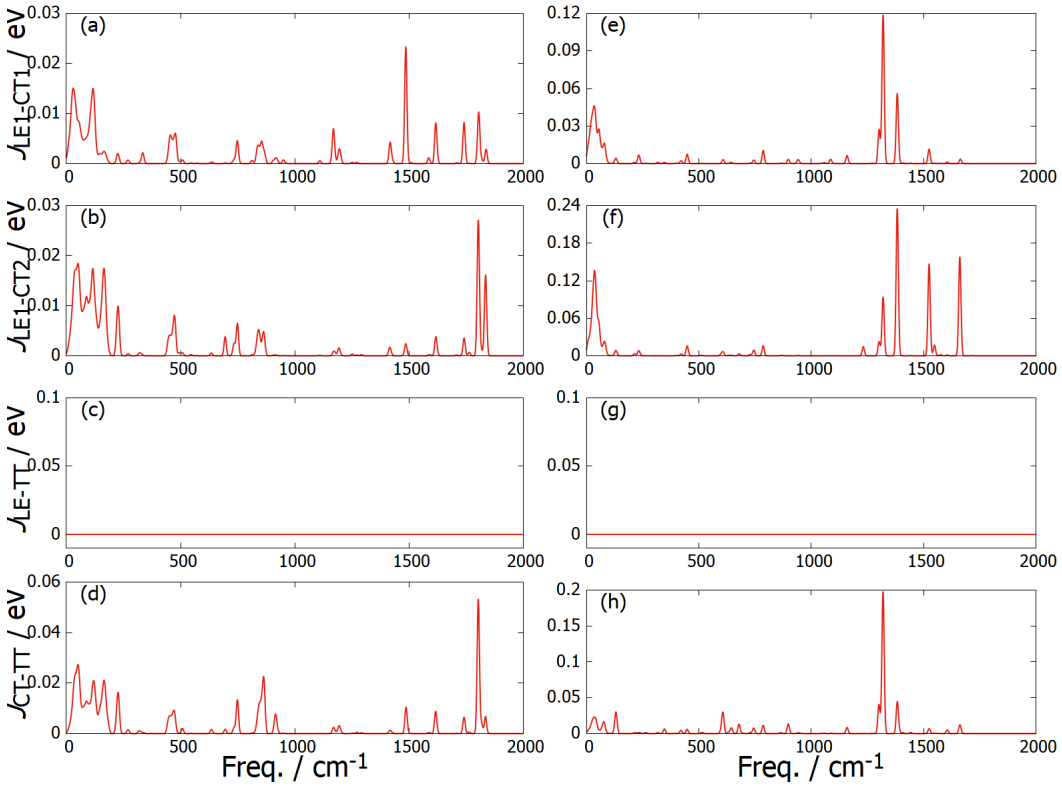

Figure 4: Spectral densities of nonlocal ex-ph couplings for tetracene dimer AB (a-d) and rubrene dimer AB (e-h). (a, e). LE1-CT1 (A^*B-A^+B^-) coupling term, (b, f). LE1-CT2 (A^*B-A^-B^+) coupling term, (c, g). LE1-TT (A^*B-A^TB^T) coupling term and (e, h) CT1-TT (A^+B^--A^TB^T) coupling term.

frequency modes also make important contributions to non-local ex-ph couplings. There are not obvious signals appeared at low-frequency range for J_{CT} which is different from previous results,[37] and this should be a consequence of different diabatization schemes as discussed in the section 3.1. The results also show that, while local ex-ph coupling can be well described by the modes of the monomers, an equally accurate description of the non-local ex-ph coupling requires accurate low frequency phonons and therefore a crystal phonon calculation.

Interestingly, in Figures 4(c) and 4(g) it is clearly shown that the spectral densities for nonlocal LE-TT couplings are nearly zero for both tetracene and rubrene systems. That is because the two-electron integrals for HOMOs and LUMOs of the two molecules determining the LE-TT couplings[3,58] are always vanishingly small, due to the fact that we used the orthonormal localized orbital set with zero orbital overlap in our diabatization scheme for each single point electronic structure calculation. Therefore, the gradient of LE-TT couplings over the vibrational modes is also negligibly small.

We also analyzed the fluctuations of electronic Hamiltonian elements (σ_i^2 for ε_i and σ_{ij}^2 for V_{ij}) at room temperature to describe the ex-ph couplings conveniently using equation below,[59]

$$\sigma_{i/ij}^2 = \int_0^\infty \mathrm{d}\omega \hbar J_{i/ij}(\omega) \coth \frac{\hbar\omega}{2k_B T}. \tag{9}$$

The computed results with room temperature (i.e. $T = 300$ K) are summarized in Tables 3 and 4. It is clearly shown that these fluctuation values for both tetracene and rubrene are mostly in the same order of magnitude at room temperature, and this could be one of the reasons for both tetracene and rubrene to exhibit SF time scales within a close range (hundreds to thousands of femtoseconds) in experiments[1,34,47,60] (unlike what one could deduce from huge differences in the symmetry in the crystal and the pure electronic parameters).

For the standard deviations of on-site energies, one may also notice that, TT state has much larger fluctuations than LE and CT states for both systems because of its double excitation characteristic (gradient of TT state energy $\nabla\varepsilon_{\mathrm{TT}}$ in SI also gives the similar

trend). For electronic coupling part, most of coupling terms in rubrene have larger values than in tetracene because of the higher distribution intensities of low frequency phonon modes and the more planar intermolecular $\pi - \pi$ stacking structure of rubrene.

It should be noted that, the nonzero spectral density and fluctuation for $V_{\mathrm{LE-CT}}$ and $V_{\mathrm{CT-TT}}$ in rubrene (Figure 4 and Table 4) implies that vibrations can activate SF in rubrene crystal, although we have shown in the above subsection that SF can hardly happen as a pure electronic effect under low temperatures due to the high symmetry crystal structure. That is because nuclear movements in some vibrational modes can break the high symmetry in equilibrium structures and accordingly $V_{\mathrm{LE-CT}}$ and $V_{\mathrm{CT-TT}}$ will become nonzero. These results are consistent with the recently proposed thermal-activated SF mechanism in rubrene crystal.[39,47] This verifies again the crucial importance of the nonlocal ex-ph couplings mainly contributed by low-frequency phonon modes.

Table 3: Fluctuation σ of electronic Hamiltonian elements of tetracene dimer AB at 300 K (unit: meV).

	A^*B	AB^*	A^+B^-	A^-B^+	A^TB^T
A^*B	234.5				
AB^*	24.4	248.2			
A^+B^-	41.3	42.6	240.3		
A^-B^+	43.0	41.3	0.037	248.8	
A^TB^T	0.025	0.084	49.2	43.9	444.4

Table 4: Fluctuation σ of electronic Hamiltonian elements of rubrene dimer AB at 300 K (unit: meV).

	A^*B	AB^*	A^+B^-	A^-B^+	A^TB^T
A^*B	238.1				
AB^*	15.4	238.1			
A^+B^-	72.1	102.2	295.3		
A^-B^+	102.2	72.1	0.012	295.0	
A^TB^T	0.055	0.055	52.8	53.0	449.2

3.3 Dynamics simulation of SF in crystalline rubrene

In this work we also simulated the SF dynamics in both crystalline tetracene and rubrene for a qualitative illustration. As discussed above, SF process in crystalline rubrene is much more complicated than in tetracene crystal and it requires activation by ex-ph couplings, therefore here we will mainly focus on the dynamics simulation for SF in rubrene. Experimentally, SF in rubrene takes places in ∼50 fs under room temperature (in frequency this is ∼600 cm^{-1})[47] , i.e. the low frequency phonon modes in Figure 4 with frequency less than 300 cm^{-1} that dominantly modulate the non-local ex-ph coupling are slower than the observed rate. Under this situation it is closer to the limit of static disorder where each conformation has a different rate because the displacement of the low frequency modes is different. It is not the common situation of Herzberg-Teller symmetry-forbidden transition[61] (where the inducing modes are still faster than the transition).

Accurate dynamics simulation of ex-ph systems with both local and nonlocal couplings is highly challenging.[3] Especially, when considering the much larger number of degrees of freedom of nuclear motion in crystal than in dimer, it would be infeasible to apply a full quantum approach for both electronic part and phonon modes and one may have to resort to Redfield theory which treats ex-ph interactions as perturbation. However it is well known that Redfield theory is problematic for dealing with very low frequency degrees of freedom,[62,63] which is dominant in our non-local ex-ph couplings. Therefore in this work we employed "Redfield theory with frozen modes" (Redfield-FM) approach recently proposed by Montoya-Castillo *et al.*[62,63] The approach consists of propagation of weak-coupling Redfield-like equations for the high-frequency bath degrees of freedom only, while the low-frequency bath modes are dynamically arrested but statistically sampled. Test results by Redfield-FM for the spin-boson model over a wide range of parameter space were found to dramatically improve Redfield dynamics in highly non-Markovian regimes, at a similar computational cost.[63]

In our case, we applied the frozen modes approach combined with the Lindblad-form

master equation[38,64] which was shown below,

$$\frac{\partial}{\partial t}\rho = -\frac{i}{\hbar}[\hat{H}_{el}, \rho] + \sum_{ij,\omega_0} \gamma_{ij}(\omega, t) \left(\hat{A}_{ij}(\omega)\rho\hat{A}_{ij}^{\dagger}(\omega) - \frac{1}{2}\{\hat{A}_{ij}^{\dagger}(\omega)\hat{A}_{ij}(\omega), \rho\} \right). \tag{10}$$

Here ρ is the reduced density matrix of electronic system, $\hat{A}_{ij}(\omega) = \sum_{E_a - E_b = \hbar\omega} |a\rangle\langle a|i\rangle\langle j|b\rangle\langle b|$ where $|a\rangle$ and $|b\rangle$ are eigenstates of $\hat{H}_{el}$ with eigenvalue E_a and E_b, And $\gamma_{ij}(\omega, t)$ is the relaxation rate which is expressed by,

$$\gamma_{ij}(\omega, t) = \int_0^{\infty} \mathrm{d}\nu J_{ij}(\nu) \left[(n(\nu) + 1)\frac{\sin(\omega - \nu)t}{\omega - \nu} + n(\nu)\frac{\sin(\omega + \nu)t}{\omega + \nu} \right], \tag{11}$$

where $n(\nu) = 1/(e^{\hbar\nu/k_B T} - 1)$ is the thermal average occupation number. Following the frozen modes approach, we treated the nonlocal ex-ph couplings as static disorder by modifying the electronic Hamiltonian with added random off-diagonal coupling terms

$$\hat{H}'_{el} = \hat{H}_{el} + \Delta V, \tag{12}$$

here ΔV are Gaussian distribution random terms with σ_{ij} calculated by Equation 9. And we only considered the diagonal terms in Equation 10 and 11 to take the local ex-ph couplings terms into account. Then the dynamics simulation was computed as statistical average of 10^4 trajectory samplings.

Figure 5 shows the time simulation results at different temperatures (30 and 300 K) with a bright initial state ($\psi_0 = \frac{1}{\sqrt{2}}(\psi_{\mathrm{LE1}} + \psi_{\mathrm{LE2}})$). The simulation results show an ultrafast temperature-enhanced singlet fission (within 100 fs) in rubrene, which agrees with recent experimental results[47] (triplet states signal appears as a result of singlet fission appear within about 40 fs). Since rate of TT state generation is controlled by electronic couplings between the CT states and TT state via super-exchange, the dynamics of SF is clearly in the conformationally gated regime where a slow degree of freedom controls the coupling (as shown in

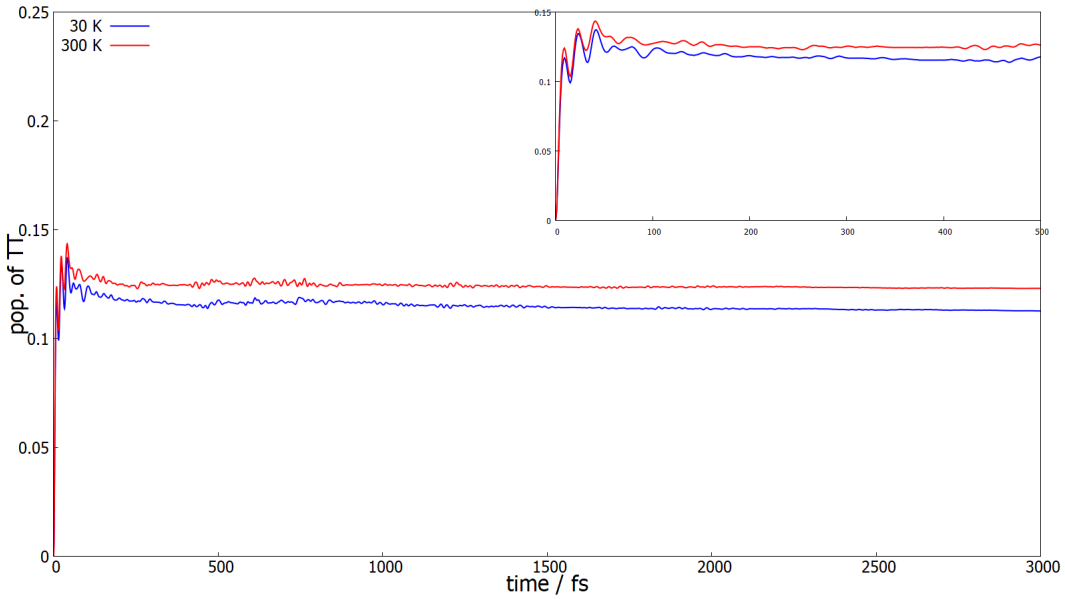

Figure 5: The dynamics results of TT population for SF of rubrene dimerAB at different temperatures within 3 ps, and the insert subfigure shows the dynamics results in the first 500 fs.

Figure 4), i.e. the rates would accordingly become non-exponential. And the population of TT state grows up with the increase of temperature with the increasing temperature from 30 K to 300 K in Figure 5 after 1 ps. We also provided the dynamics simulation results for tetracene dimerAB with a local initial state as well as the comparison results of simulation for rubrene dimer AB with other initial states (dark singlet excited state, local state) at 300 K in SI (Fig. S15 and S16 respectively). For tetracene, the population of TT state shows a near exponential evolution (∼300 fs) due to the non-zero couplings between TT state and CT states. And comparison results in Fig. S16 implies the larger TT rate and higher TT yield with a bright initial state in the time windows of 3 ps. The larger TT rate should be caused by the matching between high symmetry Hamiltonian structure and phase of bright initial states while the different yields of TT may be possibly due to the underestimation of population delay by our dynamic methods.

4 Conclusion

In this work, we built an ex-ph interaction Hamiltonian for SF in tetracene and rubrene crystal system with a full phonon description under crystalline environment. All parameters were derived from *ab initio* multi-configurational theories and semi-empirical DFTB calculations for realistic molecular dimer and crystal structures.

On the basis of this ex-ph interaction model, we studied the dynamics of SF in rubrene crystal by using a Lindblad-form master equation combining the FM approach. It is the first time for people to study local and non-local ex-ph coupling on the same footing for SF in realistic molecular crystals. Our approach explains very effectively the ultrafast SF observed for rubrene. And we also found the following points which were not known before this study:

1. The effect of non-local ex-ph coupling is to induce SF transitions in rubrene (formally symmetry forbidden) that are similar in dynamics to those in tetracene (formally symmetry allowed).

2. The modes responsible for non-local ex-ph coupling are substantially slower than the observed timescale for SF in rubrene, e.g. they can be treated as static disorders.

Our ex-ph interaction model builds a bridge linking the phenomenological descriptions of SF in dimer and oligomer approaches and microscopic modeling for phonon modes in crystals, and is accordingly expected to provide a quantitative framework for the computational study of SF process in realistic molecular crystalline environments.

Supporting Information

The Supporting Information is available free of charge on the ACS Publications website at DOI:xxx. Truncation test of gradient calculation, electronic Hamiltonian results of other dimer systems, ex-ph coupling information of rest dimer systems, and supplementary dynamic simulation results.

Acknowledgement

The work was supported by the National Natural Science Foundation of China [Grant Numbers 21673109, 21722302]. AT acknowledges funding from ERC (Grant No. 615834). We are grateful for Profs. Yi Zhao, Chunfeng Zhang and Chao-Ping Hsu for helpful discussions.

References

(1) Smith, M. B.; Michl, J. Singlet fission. *Chem. Rev.* **2010**, *110*, 6891–6936.

(2) Smith, M. B.; Michl, J. Recent advances in singlet fission. *Annu. Rev. Phys. Chem.* **2013**, *64*, 361–386.

(3) Casanova, D. Theoretical modeling of singlet fission. *Chem. Rev.* **2018**, *118*, 7164–7207.

(4) Wang, C.; Tauber, M. J. High-yield singlet fission in a zeaxanthin aggregate observed by picosecond resonance Raman spectroscopy. *J. Am. Chem. Soc.* **2010**, *132*, 13988–13991.

(5) Musser, A. J.; Al-Hashimi, M.; Maiuri, M.; Brida, D.; Heeney, M.; Cerullo, G.; Friend, R. H.; Clark, J. Activated singlet exciton fission in a semiconducting polymer. *J. Am. Chem. Soc.* **2013**, *135*, 12747–12754.

(6) Busby, E.; Xia, J.; Wu, Q.; Low, J. Z.; Song, R.; Miller, J. R.; Zhu, X.; Campos, L. M.; Sfeir, M. Y. A design strategy for intramolecular singlet fission mediated by charge-transfer states in donor–acceptor organic materials. *Nat. Mater.* **2015**, *14*, 426.

(7) Sanders, S. N.; Kumarasamy, E.; Pun, A. B.; Trinh, M. T.; Choi, B.; Xia, J.; Taffet, E. J.; Low, J. Z.; Miller, J. R.; Roy, X.; Zhu, X.-Y.; Steigerwald, M. L.; Sfeir, M. Y.; Campos, L. M. Quantitative intramolecular singlet fission in bipentacenes. *J. Am. Chem. Soc.* **2015**, *137*, 8965–8972.

(8) Zirzlmeier, J.; Lehnherr, D.; Coto, P. B.; Chernick, E. T.; Casillas, R.; Basel, B. S.; Thoss, M.; Tykwinski, R. R.; Guldi, D. M. Singlet fission in pentacene dimers. *Proc. Natl. Acad. Sci. U.S.A.* **2015**, 201422436.

(9) Sanders, S. N.; Kumarasamy, E.; Pun, A. B.; Steigerwald, M. L.; Sfeir, M. Y.; Campos, L. M. Intramolecular singlet fission in oligoacene heterodimers. *Angew. Chem.* **2016**, *128*, 3434–3438.

(10) Liu, H.; Wang, R.; Shen, L.; Xu, Y.; Xiao, M.; Zhang, C.; Li, X. A Covalently Linked Tetracene Trimer: Synthesis and Singlet Exciton Fission Property. *Org. Lett.* **2017**, *19*, 580–583.

(11) Singh, S.; Jones, W.; Siebrand, W.; Stoicheff, B.; Schneider, W. Laser generation of excitons and fluorescence in anthracene crystals. *J. Chem. Phys.* **1965**, *42*, 330–342.

(12) Hanna, M.; Nozik, A. Solar conversion efficiency of photovoltaic and photoelectrolysis cells with carrier multiplication absorbers. *J. Appl. Phys.* **2006**, *100*, 074510.

(13) Shockley, W.; Queisser, H. J. Detailed balance limit of efficiency of p-n junction solar cells. *J. Appl. Phys.* **1961**, *32*, 510–519.

(14) Zimmerman, P. M.; Zhang, Z.; Musgrave, C. B. Singlet fission in pentacene through multi-exciton quantum states. *Nat. Chem.* **2010**, *2*, 648—-652.

(15) Zimmerman, P. M.; Bell, F.; Casanova, D.; Head-Gordon, M. Mechanism for singlet fission in pentacene and tetracene: from single exciton to two triplets. *J. Am. Chem. Soc.* **2011**, *133*, 19944–19952.

(16) Havenith, R. W.; de Gier, H. D.; Broer, R. Explorative computational study of the singlet fission process. *Mol. Phys.* **2012**, *110*, 2445–2454.

(17) Casanova, D. Electronic structure study of singlet fission in tetracene derivatives. *J. Chem. Theory Comput.* **2013**, *10*, 324–334.

(18) Zeng, T.; Hoffmann, R.; Ananth, N. The low-lying electronic states of pentacene and their roles in singlet fission. *J. Am. Chem. Soc.* **2014**, *136*, 5755–5764.

(19) Parker, S. M.; Seideman, T.; Ratner, M. A.; Shiozaki, T. Model Hamiltonian analysis of singlet fission from first principles. *J. Phys. Chem. C* **2014**, *118*, 12700–12705.

(20) Coto, P. B.; Sharifzadeh, S.; Neaton, J. B.; Thoss, M. Low-lying electronic excited states of pentacene oligomers: A comparative electronic structure study in the context of singlet fission. *J. Chem. Theory Comput.* **2015**, *11*, 147–156.

(21) Ambrosio, F.; Troisi, A. Singlet fission in linear chains of molecules. *J. Chem. Phys.* **2014**, *141*, 204703.

(22) Yang, C.-H.; Hsu, C.-P. First-Principle Characterization for Singlet Fission Couplings. *J. Phys. Chem. Lett.* **2015**, *6*, 1925–1929.

(23) Mayhall, N. J. From Model Hamiltonians to ab Initio Hamiltonians and Back Again: Using Single Excitation Quantum Chemistry Methods To Find Multiexciton States in Singlet Fission Materials. *J. Chem. Theory Comput.* **2016**, *12*, 4263–4273.

(24) Ito, S.; Nagami, T.; Nakano, M. Design Principles of Electronic Couplings for Intramolecular Singlet Fission in Covalently-Linked Systems. *J. Phys. Chem. A* **2016**, *120*, 6236–6241.

(25) Ito, S.; Nagami, T.; Nakano, M. Diradical Character-Based Design for Singlet Fission of Bisanthene Derivatives: Aromatic-Ring Attachment and π-Plane Twisting. *J. Phys. Chem. Lett.* **2016**, *7*, 3925–3930.

(26) Momeni, M. R. Intramolecular Singlet Fission in Quinoidal Bi-and Tetrathiophenes: A Comparative Study of Low-Lying Excited Electronic States and Potential Energy Surfaces. *J. Chem. Theory Comput.* **2016**, *12*, 5067–5075.

(27) Zeng, T.; Goel, P. Design of small intramolecular singlet fission chromophores: an azaborine candidate and general small size effects. *J. Phys. Chem. Lett.* **2016**, *7*, 1351–1358.

(28) Ito, S.; Nagami, T.; Nakano, M. Singlet fission in pancake-bonded systems. *Phys. Chem. Chem. Phys.* **2017**, *19*, 5737–5745.

(29) Ren, J.; Peng, Q.; Zhang, X.; Yi, Y.; Shuai, Z. Role of the Dark 2Ag State in Donor–Acceptor Copolymers as a Pathway for Singlet Fission: A DMRG Study. *J. Phys. Chem. Lett.* **2017**, *8*, 2175–2181.

(30) Feng, X.; Krylov, A. I. On couplings and excimers: lessons from studies of singlet fission in covalently linked tetracene dimers. *Phys. Chem. Chem. Phys.* **2016**, *18*, 7751–7761.

(31) Refaely-Abramson, S.; Felipe, H.; Louie, S. G.; Neaton, J. B. Origins of singlet fission in solid pentacene from an ab initio Green's function approach. *Phys. Rev. Lett.* **2017**, *119*, 267401.

(32) Chan, W.-L.; Ligges, M.; Jailaubekov, A.; Kaake, L.; Miaja-Avila, L.; Zhu, X.-Y. Observing the multiexciton state in singlet fission and ensuing ultrafast multielectron transfer. *Science* **2011**, *334*, 1541–1545.

(33) Dexter, D. L. A theory of sensitized luminescence in solids. *J. Chem. Phys.* **1953**, *21*, 836–850.

(34) Chan, W.-L.; Berkelbach, T. C.; Provorse, M. R.; Monahan, N. R.; Tritsch, J. R.; Hybertsen, M. S.; Reichman, D. R.; Gao, J.; Zhu, X.-Y. The quantum coherent mechanism for singlet fission: Experiment and theory. *Acc. Chem. Res.* **2013**, *46*, 1321–1329.

(35) Beljonne, D.; Yamagata, H.; Brédas, J.; Spano, F.; Olivier, Y. Charge-transfer excitations steer the Davydov splitting and mediate singlet exciton fission in pentacene. *Phys. Rev. Lett.* **2013**, *110*, 226402.

(36) Monahan, N.; Zhu, X.-Y. Charge transfer–mediated singlet fission. *Annu. Rev. Phys. Chem.* **2015**, *66*, 601–618.

(37) Ito, S.; Nagami, T.; Nakano, M. Density analysis of intra-and intermolecular vibronic couplings toward bath engineering for singlet fission. *The journal of physical chemistry letters* **2015**, *6*, 4972–4977.

(38) Renaud, N.; Grozema, F. C. Intermolecular vibrational modes speed up singlet fission in perylenediimide crystals. *J. Phys. Chem. Lett.* **2015**, *6*, 360–365.

(39) Tamura, H.; Huix-Rotllant, M.; Burghardt, I.; Olivier, Y.; Beljonne, D. First-principles quantum dynamics of singlet fission: coherent versus thermally activated mechanisms governed by molecular π stacking. *Phys. Rev. Lett.* **2015**, *115*, 107401.

(40) Yao, Y. Coherent dynamics of singlet fission controlled by nonlocal electron-phonon coupling. *Phys. Rev. B* **2016**, *93*, 115426.

(41) Fujihashi, Y.; Ishizaki, A. Fluctuations in electronic energy affecting singlet fission dynamics and mixing with charge-transfer state: quantum dynamics study. *J. Phys. Chem. Lett.* **2016**, *7*, 363–369.

(42) Nakano, M.; Ito, S.; Nagami, T.; Kitagawa, Y.; Kubo, T. Quantum Master Equation Approach to Singlet Fission Dynamics of Realistic/Artificial Pentacene Dimer Models: Relative Relaxation Factor Analysis. *J. Phys. Chem. C* **2016**, *120*, 22803–22815.

(43) Stern, H. L.; Cheminal, A.; Yost, S. R.; Broch, K.; Bayliss, S. L.; Chen, K.; Tabachnyk, M.; Thorley, K.; Greenham, N.; Hodgkiss, J. M.; Anthony, J.; Head-Gordon, M.; Musser, A. J.; Rao, A.; Friend, R. H. Vibronically coherent ultrafast triplet-pair formation and subsequent thermally activated dissociation control efficient endothermic singlet fission. *Nat. Chem.* **2017**, *9*, 1205.

(44) Morrison, A. F.; Herbert, J. M. Evidence for singlet fission driven by vibronic coherence in crystalline tetracene. *J. Phys. Chem. Lett.* **2017**, *8*, 1442–1448.

(45) Zang, H.; Zhao, Y.; Liang, W. Quantum Interference in Singlet Fission: J-and H-Aggregate Behavior. *J. Phys. Chem. Lett.* **2017**, *8*, 5105–5112.

(46) Monahan, N. R.; Sun, D.; Tamura, H.; Williams, K. W.; Xu, B.; Zhong, Y.; Kumar, B.; Nuckolls, C.; Harutyunyan, A. R.; Chen, G.; Dai, H.-L.; Beljonne, D.; Rao, Y.; Zhu, X.-

Y. Dynamics of the triplet-pair state reveals the likely coexistence of coherent and incoherent singlet fission in crystalline hexacene. *Nat. Chem.* **2017**, *9*, 341.

(47) Miyata, K.; Kurashige, Y.; Watanabe, K.; Sugimoto, T.; Takahashi, S.; Tanaka, S.; Takeya, J.; Yanai, T.; Matsumoto, Y. Coherent singlet fission activated by symmetry breaking. *Nat. Chem.* **2017**, *9*, 983.

(48) Zheng, J.; Xie, Y.; Jiang, S.; Lan, Z. Ultrafast Nonadiabatic Dynamics of Singlet Fission: Quantum Dynamics with the Multilayer Multiconfigurational Time-Dependent Hartree (ML-MCTDH) Method. *J. Phys. Chem. C* **2016**, *120*, 1375–1389.

(49) Reddy, S. R.; Coto, P. B.; Thoss, M. Intramolecular Singlet Fission: Insights from Quantum Dynamical Simulations. *J. Phys. Chem. Lett.* **2018**, *9*, 5979–5986.

(50) Wang, L.; Olivier, Y.; Prezhdo, O. V.; Beljonne, D. Maximizing singlet fission by intermolecular packing. *J. Phys. Chem. Lett.* **2014**, *5*, 3345–3353.

(51) Xie, X.; Santana-Bonilla, A.; Troisi, A. Nonlocal Electron–Phonon Coupling in Prototypical Molecular Semiconductors from First Principles. *J. Chem. Theory Comput.* **2018**, *14*, 3752–3762.

(52) Wilson, M. W.; Rao, A.; Johnson, K.; Gélinas, S.; Di Pietro, R.; Clark, J.; Friend, R. H. Temperature-independent singlet exciton fission in tetracene. *J. Am. Chem. Soc.* **2013**, *135*, 16680–16688.

(53) Aquilante, F.; Autschbach, J.; Carlson, R. K.; Chibotaru, L. F.; Delcey, M. G.; De Vico, L.; Fdez. Galván, I.; Ferrè, N.; Frutos, L. M.; Gagliardi, L.; Garavelli, M.; Giussani, A.; Hoyer, C. E.; Li Manni, G.; Lischka, H.; Ma, D.; Malmqvist, P. Å.; Müller, T.; Nenov, A.; Olivucci, M.; Pedersen, T. B.; Peng, D.; Plasser, F.; Pritchard, B.; Reiher, M.; Rivalta, I.; Schapiro, I.; Segarra-Martí, J.; Stenrup, M.; Truhlar, D. G.; Ungur, L.; Valentini, A.; Vancoillie, S.; Veryazov, V.; Vysotskiy, V. P.; Weingart, O.;

Zapata, F.; Lindh, R. Molcas 8: New capabilities for multiconfigurational quantum chemical calculations across the periodic table. *J. Comput. Chem.* **2016**, *37*, 506–541.

(54) Löwdin, P.-O. *Advances in quantum chemistry*; Elsevier, 1970; Vol. 5; pp 185–199.

(55) Holmes, D.; Kumaraswamy, S.; Matzger, A. J.; Vollhardt, K. P. C. On the Nature of Nonplanarity in the [N]Phenylenes. *Chem. Eur. J.* **1999**, *5*, 3399–3412.

(56) Jurchescu, O. D.; Meetsma, A.; Palstra, T. T. M. Low-temperature structure of rubrene single crystals grown by vapor transport. *Acta Cryst. B* **2006**, *62*, 330–334.

(57) da Silva Filho, D. A.; Kim, E.-G.; Brédas, J.-L. Transport properties in the rubrene crystal: electronic coupling and vibrational reorganization energy. *Advanced Materials* **2005**, *17*, 1072–1076.

(58) Buchanan, E. A.; Michl, J. Packing Guidelines for Optimizing Singlet Fission Matrix Elements in Noncovalent Dimers. *J. Am. Chem. Soc.* **2017**, *139*, 15572–15575.

(59) Coropceanu, V.; Sánchez-Carrera, R. S.; Paramonov, P.; Day, G. M.; Brédas, J.-L. Interaction of charge carriers with lattice vibrations in organic molecular semiconductors: naphthalene as a case study. *J. Phys. Chem. C* **2009**, *113*, 4679–4686.

(60) Chan, W.-L.; Ligges, M.; Zhu, X. The energy barrier in singlet fission can be overcome through coherent coupling and entropic gain. *Nat. Chem.* **2012**, *4*, 840.

(61) Herzberg, G.; Teller, E. Schwingungsstruktur der Elektronenübergänge bei mehratomigen Molekülen. *Zeitschrift für Physikalische Chemie* **1933**, *21*, 410–446.

(62) Montoya-Castillo, A.; Berkelbach, T. C.; Reichman, D. R. Extending the applicability of Redfield theories into highly non-Markovian regimes. *J. Chem. Phys.* **2015**, *143*, 194108.

(63) Tempelaar, R.; Reichman, D. R. Vibronic exciton theory of singlet fission. III. How vibronic coupling and thermodynamics promote rapid triplet generation in pentacene crystals. *J. Chem. Phys.* **2018**, *148*, 244701.

(64) Breuer, H. P.; Petruccione, F. *The theory of open quantum systems*; Oxford University Press: Great Clarendon Street, 2002.

5 TOC